Published in final edited form as:

Fertil Steril. 2016 April ; 105(4): 1023–1034. doi:10.1016/j.fertnstert.2015.11.045.

A western-style diet, with and without chronic androgen treatment, alters the number, structure and function of small antral follicles in ovaries of young adult monkeys

Cecily V. Bishop, PhD[1,5], **Fuhua Xu, PhD.**[1], **Jing Xu, PhD.**[1], **Alison Y. Ting, PhD**[1], **Etienne Galbreath, B.S.**[1], **Whitney K. McGee, DVM, PhD**[2], **Mary B. Zelinski, PhD**[1], **Jon D. Hennebold, PhD**[1,3], **Judy L. Cameron, PhD**[2,4], and **Richard L. Stouffer, PhD**[1,3]

[1]Division of Reproductive & Developmental Sciences, Oregon National Primate Research Center, Beaverton, OR, USA, 97006

[2]Department of Behavioral Neuroscience, Oregon Health & Science University, Portland, OR, USA, 97239

[3]Department of Obstectrics & Gynecology, Oregon Health & Science University, Portland, OR, USA, 97239

[4]Department of Psychiatry, University of Pittsburgh, Pittsburgh, PA, 15213, USA

Abstract

Objective—To examine the small antral follicle (SAF) cohort in ovaries of adult rhesus monkeys following consumption of a western-style diet (WSD), with or without chronically elevated androgen levels since before puberty.

Design—Cholesterol or testosterone (T; n=6/group) implants were placed subcutaneously in female rhesus macaques beginning at 1 yr of age (pre-pubertal), with addition of a WSD (high fat/fructose) at 5.5 yrs (menarche ~2.6 yrs). Ovaries were collected at 7 yrs of age. One ovary/female was embedded in paraffin for morphological and immunohistochemical analyses. The SAFs (<2.5mm) were dissected from the other ovary obtained at/near menses in a subgroup of females (n=3/group), and processed for microarray analyses of the SAF transcriptome. Ovaries of adult monkeys consuming a standard macaque diet (low in fats and sugars) were obtained at similar stages of the menstrual cycle and used as controls for all analyses.

Setting—National primate research center

Animals—Adult, female rhesus monkeys (*Macaca mulatta*)

Interventions—None

[5]Corresponding Author, Cecily V. Bishop, Ph.D., Division of Reproductive & Developmental Sciences, Oregon National Primate Research Center, 505 NW 185th Ave, Beaverton, OR 97006. bishopc@ohsu.edu; 1-503-533-2422.

Conflict of Interest: All authors declare they have no conflict of interest as it pertains to the data presented in this manuscript.

Main outcome measures—Histological analyses, SAF counts and morphology, protein localization and abundance in SAFs, transcriptome in SAFs (mRNAs)

Results—Compared to controls, consumption of a WSD, with and without T treatment, increased the numbers of SAFs per ovary, due to the presence of more atretic follicles. Numbers of granulosa cells expressing cellular proliferation markers (pRb and pH3) was greater in healthy SAFs, while numbers of cells expressing the cell cycle inhibitor (p21) was higher in atretic SAFs. Intense CYP17A1 staining was observed in the theca cells of SAFs from WSD+/− T groups, compared to controls. Microarray analyses of the transcriptome in SAFs isolated from WSD and WSD+T treated females and controls consuming a standard diet, identified 1944 genes whose mRNA levels changed ≥2-fold among the three groups. Further analyses identified several gene pathways altered by WSD and/or WSD+T associated with steroid, carbohydrate and lipid metabolism, plus ovarian processes. Alterations in levels of several SAF mRNAs are similar to those observed in follicular cells from women with polycystic ovary syndrome (PCOS).

Conclusion—These data indicate that consumption of a WSD high in fats and sugars in the presence and absence of chronically elevated T alters the structure and function of SAFs within primate ovaries.

Keywords

Small Antral Follicles; Metabolism; Androgen; Western-Style Diet; Ovarian Function

Introduction

The disorder polycystic ovary syndrome (PCOS) is a major cause of infertility in women. The main characteristics of women with PCOS include elevated androgen levels, hirsutism, and alterations to the hypothalamic-pituitary-ovarian (HPO) axis manifesting in oligo- or anovulation and polycystic ovary morphology (1). The ovarian morphology of many women with a clinical diagnosis of PCOS is multi-follicular; the current guidelines from the Androgen Excess and PCOS Society indicate that ≥25 small to medium sized (<10 mm) antral follicles (SAFs) in each ovary is sufficient for diagnosis of PCO morphology (PCOM) by ultrasonography (2). Classically, these SAFs are observed in the periphery of the ovary, leading to the “string of pearls” appearance (3). Growth of these follicles is typically arrested at the small antral stage, and they may persist as cystic structures even after degeneration of granulosa cells lining the interior of the follicle (4).

There is also a high incidence of obesity in women with PCOS, leading to an altered metabolic state including increased prevalence of insulin resistance and development of metabolic syndrome (5, 6) compared to individuals with a lean PCOS phenotype. Obesity alone imparts a well-documented detrimental impact on a woman’s health (7), and research is now focusing on the impact of alterations to the metabolic state on fertility and the contribution of obesity to onset and severity of PCOS phenotype (8).

The mechanism(s) leading to development of a PCOS phenotype are currently unclear and, due to the heterogeneous nature of the disorder, are likely multifaceted. However, exposure of female monkeys and sheep to exogenously elevated androgens in utero can cause a

PCOS-like phenotype which manifests in the offspring during adulthood (9, 10). We recently developed a nonhuman primate model to test the hypothesis that a 3–4 fold elevation in circulating testosterone (T) levels, beginning prior to/during puberty leads to development of symptoms associated with PCOS in young adults. This model recapitulates the scenario when endogenous T levels begin to rise in adolescent girls at risk for PCOS (1). Female macaques received silastic implants containing cholesterol or T beginning at 1 year of age (11, 12). Chronic exposure to elevated T levels altered hypothalamic-pituitary function by 4 years of age (increased LH pulse frequency), similar to reported alterations observed in adolescents with PCOS, but there was no major effect on ovarian morphology/function in these peripubertal monkeys (11).

Given the strong association between PCOS and metabolism, it was postulated that addition of a western-style diet (high-fat and fructose; WSD) and subsequent changes in metabolism would induce or exacerbate PCOS-like symptoms. Thus, a WSD was fed to these control and T-treated females beginning at 5.5 years of age until the end of the study, 1.5 years later (12). The WSD increased body weight and % body fat in all females (12, 13). Reduced sensitivity to insulin was observed in females receiving both WSD and T, but not with WSD alone (12). All females displayed reduced levels of estradiol (E) and shorter follicular phases compared to before onset of WSD, but evidence of ovulatory activity was detected in these females based on patterns of E and progesterone (P) secretion (12). Ovarian ultrasonography performed at menstruation observed increased numbers of small antral follicles in all females when compared to before onset of WSD. Larger numbers of small, non-ovulatory antral follicles (“subordinate antral follicles”; approx. 7) were also detected at late follicular phase in WSD-exposed females compared to those (3–4 subordinates) of adult rhesus monkeys consuming a standard diet (14). The size of the largest (putatively dominant) antral follicle was also markedly less in WSD+/−T animals than in controls (12).

Due to the observed alterations in the ovarian phenotype induced by WSD (+/−) T of these macaque females (12), the ovaries were collected from these females to 1) histologically analyze the impact of WSD with and without chronically elevated T on the small antral follicle (SAF) cohort in the ovary, and 2) characterize alterations to the SAF transcriptome. These data were compared to that obtained from control monkeys in our colony, i.e., adult macaques with regular menstrual cycles receiving a standard low-fat/low-sugar diet, and without chronic elevation of androgens.

Materials and Methods

Animals

All procedures were reviewed and approved by the Oregon Health & Science University/Oregon National Primate Research Center Institutional Animal Care and Use Committee. A cohort of female rhesus monkeys (*Macaca mulatta*; n=6/treatment group), detailed in McGee et al (11, 12), received silastic implants containing either cholesterol or testosterone (T); the latter maintained a 3–4 fold elevation of circulating T from 1 year of age until the end of the study (pre-pubertal to adult). From 1 until 5.5 years of age, females consumed a standard diet (15% calories from fat, 27% from protein, 59% from carbohydrates; no. 5000; Purina Mills Co., St. Louis, MO), supplemented with fresh fruits and vegetables. Then, at 5.5 years

of age, these females were transitioned to a western-style diet (WSD: 33% calories from fat, 17% from protein, 51% from carbohydrates; 5A1F, Purina Mills, St. Louis, MO) supplemented with high-fructose treats (12, 13), which they consumed until the end of the study (~7 years old).

At the end of the study, WSD with and without chronic T-exposure (+/− T) females were randomly divided into two subgroups for ovarian collection: either at menses (early follicular phase, days 1–3 of the menstrual cycle; onset of frank menses = day 1, n=3/ group) or at mid-luteal phase (n=3/group). There were no differences in serum E levels between WSD and WSD+T females collected at menses, but WSD+T females had reduced mid-luteal phase serum P levels compared to WSD alone (13). Ovaries were collected from anesthetized females as previously described (15).

One ovary per female was selected for fixation: either randomly from females at/near onset of menses, or the non-corpus luteum (CL)-bearing ovary from the luteal phase of the menstrual cycle, and processed as described below (histological evaluation). Ovaries at these stages of the menstrual cycle were also obtained from adult macaques with regular menstrual cycles (7.3±0.5 years of age; control), either as whole tissue (n=3) or pre-stained hematoxylin and eosin (H&E) tissue sections on glass permafrost slides (n=4), via the ONPRC Tissue Distribution Program and processed as described below. These control females consumed the standard low-fat/low-sugar macaque diet (no. 5000; Purina Mills Co.) described earlier.

Small antral follicles (SAFs) were dissected from the remaining ovary of a subset of WSD +/− T females collected at onset of menses (n=3/group) under a light dissecting microscope as previously described (16) and detailed below (SAF transcriptome). Ovaries of adult rhesus monkeys with regular menstrual cycles consuming the standard macaque diet described above (11.8±0.5 years of age, n=3) collected at/near onset of menses, were obtained from the ONPRC Tissue Distribution Program. The SAFs were dissected from the stroma of these ovaries as detailed below to serve as controls (SAF transcriptome).

Histological evaluation

All chemicals were obtained from Sigma-Aldrich, USA unless noted. Whole ovaries were fixed in 10% neutral-buffered formalin (v/v; Richard-Allen Scientific; Thermo Scientific, Inc, USA) for 24 hr at 4°C. Then the buffer was replaced with PBS containing 10% sucralose, and tissue incubated another 24 hr at 4°C until processed for paraffin embedding. Serial 5μm sections were prepared from the entire ovary, and placed on permafrost slides (3 sections/slide). Following paraffin removal and re-hydration by incubation in D-Limonene Clearant (VWR International, LLC, USA), 100% and 70% ethanol, and deionized water, selected slides containing ovarian sections were processed for either H&E staining or immunohistochemistry.

H&E Staining—Slides containing tissue sections at/near the greatest diameter of ovary (n=6 ovaries/ treatment group) were incubated in hematoxylin, followed by acid alcohol (1% in ethanol), and lithium carbonate per manufacturer protocols (17). Slides were then counterstained with eosin, dehydrated in ethanol and D-Limonene Clearant, and cover slips

adhered with an aqueous mounting medium (DPX). Small antral follicles (SAFs) were noted to be healthy or atretic from morphology of the granulosa cell layer, based on similar histological evaluation of total SAFs in women with PCOS (18). The number of healthy and atretic SAFs were counted in 3 sections/ ovary using Cell Counter add-on of ImageJ (NCBI) and then averaged to estimate the number of healthy and atretic SAFs/ovary.

Immunohistochemistry—IHC was performed on selected ovarian sections from treatment groups (WSD+/− T; n=6 ovaries each) and from standard diet controls (n=3 ovaries) for proteins involved in cell-proliferation [phosphorylated retinoblastoma 1 (pRb) and histone cluster 3 H3 (pH3)], cell-cycle inhibition (cyclin-dependent kinase inhibitor 1A/ CDKN1A; p21), and theca cell steroidogenesis (cytochrome P450, family 17, subfamily A, polypeptide 1; CYP17A1). Heated Citrate Buffer Antigen Retrieval (pressure cooker method) was performed to break formalin-induced protein cross-links and unmask antigenic sites (17). Sections were then incubated for 24 hr at 4°C in blocking buffer containing 1% BSA/PBS (pRb, pH3, and p21) or 10% normal goat serum (CYP17A1) to reduce non-specific binding. The sections were incubated for another 24 hr at 4°C in either primary antibody of interest [anti-human pRb and p21, Cell Signaling Technology; anti-human pH3, Chemicon International (17); anti-human CYP17A1, provided by Dr. Alan J. Conley, University of California, Davis, CA, USA (19)], or were maintained in blocking buffer to correct for nonspecific interactions of secondary antibody. Antibody binding was visualized as previously reported for macaque tissues (17, 19). Sections were counterstained with either nuclear fast red or hematoxylin, dehydrated in ethanol and D-Limonene Clearant, and cover slips adhered with DPX mounting medium.

Immunostaining for pRb, pH3, and p21 was analyzed by comparing the number of positively staining granulosa cells within a SAF, as a percentage of total granulosa cells per SAF, in all SAFs within an ovarian section using ImageJ software (Cell Counter add-on) after subtraction of nonspecific staining (controlled false-positive rate/SAF; average of 3 sections/ ovary); data were segregated into SAF type i.e. healthy or atretic by granulosa cell layer morphology. Width of the theca layer of healthy SAF (>0.5 mm diameter) was denoted from CYP17A1 staining; the width of positive (dark brown) staining over 5 randomly selected areas surrounding the SAF was measured using the straight line function of ImageJ and averaged (n= 3 healthy SAFs/ovary/ treatment group).

Ultrasound evaluation of ovarian structure—Archived ultrasound image files from WSD+/−T treated females (as reported in (12)) were analyzed to relate to ovarian SAF morphology from histologic analyses. Image files were from scans performed on days 1–3 of the menstrual cycle at three separate time points: a) before onset of WSD, b) 3 months, and d) 14 months after onset of WSD exposure. Females were approximately 5.0, 5.8, and 6.7 years of age, respectively. Archived ultrasound scans were also analyzed from adult rhesus females with regular menstrual cycles consuming the standard monkey chow diet (control), undergoing similar ultrasound evaluation of ovarian structure for an unrelated project on days 1–3 of the menstrual cycle (standard diet control; 7 ± 2 years; n=13). GE Voluson 730 Expert Image files from each ultrasound session were coded to mask identifying information, uploaded into 4D View software (GE Healthcare, Milwaukee, WI,

USA), and analyzed at one time by a single individual (CVB), similar to previous analyses (12). Localization of the majority of SAFs (<2.5 mm) to the outer periphery of the ovary was denoted as polycystic ovary morphology (PCOM). All scans were then decoded for comparisons between treatment groups.

SAF transcriptome

Presumptive healthy SAFs were chosen for transcriptome evaluation based on criteria reported previously (16): the presence of a clear antrum lacking dark oocytes or granulosa cells. Isolated healthy SAFs from an ovary were pooled (3.7±0.3 SAFs/ovary), cleaned of extraneous stroma using 30-gauge needles, ruptured, and entire cellular contents (follicle wall/granulosa cells and cumulus-oocyte complex) placed into lysis buffer for RNA isolation (Absolutely RNA Nanoprep Kit, Agilent Technologies, Inc. USA). Purified SAF RNA from each ovary (n=3 ovaries/treatment group) was hybridized to individual Affymetrix™ GeneChip Rhesus Macaque Genome Arrays by the OHSU Gene Profiling Shared Resource (GPSR), similar to previous macaque microarray studies (20). Hybridization protocols were performed by the OHSU GPSR (21). Data are publically available as a NCBI GEO data set (http://www.ncbi.nlm.nih.gov/gds, Series GSE69716).

Microarray data were validated by selecting a subset of mRNAs displaying different patterns of expression in SAFs as a function of treatments. Aliquots of SAF RNA from each ovary were reverse-transcribed into cDNA (GoScript™ Reverse Transcription System, Promega, USA), and quantitative real-time PCR analysis was performed as previously described (22) on selected gene products using TaqMan® Gene Expression Assays (Applied Biosystems®, USA; Supplemental Table 1).

Statistics

All SAF counts and protein staining (% positive granulosa cells) were analyzed using the generalized linear modeling (GLM) procedure of SAS (9.3), comparing ovaries from WSD +/−T females and standard diet controls. Significant differences between treatments were determined by least-squares means function. Presence of PCOM in at least one ovary from WSD-fed +/− T females was analyzed by Wilcoxon Rank-Sum Test (SAS version 9.3, SAS Institute Inc. USA).

Processed microarray image (.CEL) files were analyzed using the web-based GeneSifter® software (Geospiza, Inc., Seattle, WA, USA) and probeset (mRNA) hybridization data were log2-transformed using the Robust Multi-array Average (RMA) algorithm as previously reported (23). All mRNA expression data were interrogated by one-way ANOVA; standard diet (control) versus WSD versus WSD+T (n=3/ group). Significant change in mRNA levels was defined as a ≥2-fold difference after false-discovery rate correction (FDR; Benjamini and Hochberg, $P < 0.05$). Pairwise comparisons were performed on SAF mRNA levels between standard diet controls, WSD, and WSD+T by Welch's T-test (≥2 fold, $P<0.05$). KEGG analysis was performed on the list of significantly altered mRNAs similar to previous methods (23). Significant ontologies identified by GeneSifter were refined by eliminating those in which fewer than 5 gene products were associated with the ontology (too narrow classification), and with greater than 100 gene products (too broad) similar to Doniger et al

(24). All non-significant ontologies with z-scores less than 2.0 were also eliminated as previously reported (25). All real-time qPCR data were analyzed by one-way ANOVA and log2-transformed to correct for heterogeneity of variances if needed (SAS®, 9.3).

Results

Ovarian Morphology/ Histology

Morphology by H&E staining—Compared to ovaries collected at menstruation from control macaques consuming a standard diet (Figure 1A), those from both WSD (1 B) and WSD+T (1 C) treated monkeys displayed numerous SAFs and several regressing luteal-like structures.

Morphology by ultrasound—We previously reported transabdominal ultrasound evaluation of the SAF cohort in WSD+/−T ovaries near onset of menses; the total number of SAFs increased after the onset of WSD in both treatment groups, with a concurrent decrease in average diameter (12). Typically rhesus ovaries have SAFs localized throughout the ovary as indicated by dark echogenic areas on ultrasound images (Supplemental Figure 1A). However, the current analyses determined that many WSD+/−T exposed-monkeys displayed compartmentalization of the SAF in the periphery of the ovary, resulting in polycystic ovary-like morphology (PCOM; Supplemental Figure 1B–C), in agreement with histological evaluation of several WSD +/−T ovaries by H&E staining (example Figure 1C). Prior to the onset of WSD, 2 of 6 cholesterol-treated females had a least one ovary showing PCOM, compared to 3 of 6 T-treated females as judged by ultrasound evaluation (Supplemental Table 2). Two months after introduction of the WSD, all 6 WSD+T females displayed PCOM by ultrasound in at least one ovary (P=0.01 vs WSD alone); this morphology was noted again in all WSD+T females at 6.7 years of age. The number of WSD-treated females presenting with PCOM after 2 months of WSD increased to 3. By the end of treatment, 5 of 6 WSD-treated females presented with PCOM in at least 1 ovary, and there was no longer any difference between morphology compared to WSD+T exposure; 11 of 12 WSD+/−T treated females displayed at least one ovary with PCOM, resulting in a prevalence of 92%. Notably, ultrasound evaluation of standard diet controls revealed PCOM in at least one ovary in 4 of 13 rhesus females, resulting in an estimated prevalence of 30% in monkeys consuming a standard chow diet.

SAF cohort—When healthy and atretic SAFs were evaluated in H&E-stained cross-sections from ovaries (e.g., Figs 2A and B), the estimated number of SAFs in ovaries from WSD and WSD+T treated macaques was greater compared to ovaries from animals consuming the standard low-fat diet (Figure 1D; P<0.001, 0.02, respectively). This was primarily due to greater numbers of atretic SAFs present in ovaries from the WSD and WSD +T groups (P<0.001). The number of healthy SAFs in ovaries from WSD-alone females tended (P=0.06) to be greater than in standard diet controls. However, the number of healthy SAFs in ovaries of WSD+T was not different from either controls or WSD-only (P>0.05, 0.2, respectively). Also, there were no differences within treatment groups in SAF populations of ovaries collected at menstruation versus the non-dominant ovary of mid-luteal phase (P>0.4, data not shown).

Immunohistochemistry—A 6.3-fold greater percentage of granulosa cells in atretic SAFs stained for p21 compared to healthy SAFs (Figure 2, panels A–B; P<0.001). In contrast, a 12-fold greater percentage of granulosa cells stained for pRb in healthy compared to atretic SAFs (Figure 2, panels C–D; P<0.0001). A similar increase in granulosa cells immunostaining for pH3 was noted in heathy versus atretic SAFs (data not shown). However, there were no significant differences in percentage of granulosa cells with positive staining for any of these cellular markers between either healthy or atretic SAFs in ovaries from control versus WSD+/− T treated monkeys (data not shown).

Immunostaining for CYP17A1 was used to identify and estimate the thickness of the theca layer of healthy SAFs (Figure 2, Panels E–G). The theca layer of healthy SAFs in ovaries of WSD and WSD+T females displayed more intense staining for CYP17A1 than in control ovaries. Healthy SAFs in ovaries from WSD+T-treated monkeys had a 25% thicker theca cell layer compared to those of standard diet controls (Figure 2H; P<0.05). However the theca layer of healthy SAFs in ovaries of WSD-treated monkeys was not thicker than those in ovaries of control females (P>0.5).

SAF Transcriptome

Microarray analyses—The levels of 1944 mRNAs were significantly altered in SAFs by WSD+/− T compared to controls (One way ANOVA, ≥2-fold change in expression with FDR, P<0.05; Supplemental File 1). A heat map of mRNAs whose levels were altered by treatment is depicted in Figure 3A. When k-Medoids clustering of mRNA expression patterns between standard diet control, WSD and WSD+T was performed using GeneSifter (Figure 3B), 8 distinct patterns were identified. Pattern 7 depicts a cohort of mRNAs increased by T-exposure alone, and Pattern 8 is decreased by T-exposure. Patterns 2 and 5 depict mRNA cohorts increased/decreased by exposure to WSD, with no additional effects of T-exposure. However, expression Patterns 1, 3, 4 and 6 show partial negation of the stimulatory or inhibitory effects of WSD on mRNA levels by T-exposure. Hierarchical clustering (Figure 3C) and PCA (Supplemental Figure 2) confirmed that both WSD and WSD+T distinctly alter the transcriptome of SAFs compared to controls. Pairwise analyses (Figure 3D; Supplemental Files 2–4) confirmed the k-Medoids clustering, demonstrating divergent mRNA expression patterns between those SAFs isolated from standard diet control and WSD+/−T.

KEGG analyses performed on mRNAs significantly altered in SAFs of treated females (from Supplemental File 1) identified several pathways containing gene activity altered by WSD +/− T (Supplemental Tables 3–4). The most impacted pathway (by z-score analysis of statistical significance) is DNA replication, followed by cell cycle and mismatch repair. Genes found in pathways associated with classical reproductive processes are also noted; GnRH signaling, steroid hormone biosynthesis and progesterone-mediated oocyte maturation. Several pathways involved in cancer, apoptosis, and inflammatory responses (i.e. autoimmune thyroid disease), are also altered in SAFs by WSD +/− T.

Gene ontology analyses of mRNAs significantly altered in SAFs by treatments (from Supplemental File 1) were mined with Gene Sifter. Gene products from ontologies broadly associated with carbohydrate, lipid metabolism and steroid metabolic processes were

impacted by exposure to both WSD and chronically elevated T (Supplemental Figure 3A–C). Narrowing these broad categories to significant sub-ontologies (26) identified a number of tissue processes altered by WSD and WSD+T (Supplemental File 5) including gene products associated with angiogenesis, oogenesis, and inflammatory response (Supplemental Figure 4A–C). While mRNAs in angiogenesis and inflammatory response are mostly increased by WSD and WSD+T treatment, those in oogenesis were primarily suppressed by WSD+/−T. Also, many mRNAs depicted in Supplemental Figures 3 and 4 are altered by WSD exposure alone, and several are altered by exposure to WSD+T but not WSD alone.

All mRNAs present in the RMA-transformed SAF microarray database (Supplemental Files 6–8) were also mined for gene products classically associated with ovarian function and metabolism, as well as oocyte factors altered by obesity in women (27), and select mRNAs differentially expressed in granulosa and cultured cumulus cells from antral follicles of women with and without PCOS undergoing IVF protocols (28, 29) [http://www.ncbi.nlm.nih.gov/geoprofiles/GEO Accession #s GDS4399 (granulosa cell) and GDS3841(cultured cumulus cells, subdivided into lean and obese phenotype)]. Of the 34 gene products interrogated (Supplemental Table 5), 26 demonstrate significant alterations in mRNA levels following WSD and/or WSD+T, including AMH, ANGPT2, AR, CYP19A1, ESR1, FSHR, LHCGR, PGRMC1, INSLR, DDIT3, HSPA5, FADS1, PTPLA, and SC4MOL.

Real-time PCR validation—Several gene products were chosen for validation based on relevance to follicular development (Figure 4): *CYP17A1* mRNA levels were reduced by addition of the WSD and not further impacted by T exposure (Figure 4A, similar to Figure 3 Pattern 2), *HSD3B2* mRNA levels were reduced by WSD and further suppressed by chronic T exposure (Figure 4B, similar to Figure 3 Pattern 8), levels of *LHCGR* mRNA were significantly reduced by WSD and restored to control levels by T exposure (Figure 4C, similar to Figure 3 Pattern 6), and expression of *PGR* was not significantly impacted by either WSD or T (Figure 4D). Expression patterns were similar between real-time PCR and microarray analyses, if not statistically significant.

Discussion

Previous ultrasound evaluation of this cohort of females performed during the early follicular phase revealed increasing numbers of SAFs in the ovaries of both WSD and WSD +T groups, and a subsequent reduction in maximum follicle diameter compared to before onset of the WSD (12). Moreover, WSD + T treatment resulted in greater number of SAFs and a lead follicle of smaller diameter in the late follicular phase, as well as reduced peak levels of P circulating in the luteal phase, compared to WSD alone. Histological evaluations in the current study (Figure 1) are consistent with these earlier findings: ovaries from WSD +/− T-treated females have larger numbers of SAFs in the early follicular phase, primarily due to an increased number of atretic SAFs compared to females consuming a standard low-fat, low-sugar diet. The ultrasound and histological data also suggest alterations to the localization of SAFs, following WSD+/−T treatment. One of the most striking features of women with polycystic ovary syndrome is the presence of numerous small to medium (<10mm) antral follicles that persist on the periphery of the ovary, the so-called PCOM (2);

there is evidence that these antral follicles slowly degenerate across several menstrual cycles (4). Prior to introduction of the WSD, T-exposed females began to exhibit a PCOM-like phenotype in at least 1 ovary at a greater rate than cholesterol-treated females (Supplemental Table 2). After addition of the WSD, ovaries of both treatment groups displayed PCOM, although more prevalent at first in T-treated animals. Notably, 30% of standard diet, control females also exhibited a PCOM-like phenotype upon ultrasound evaluation. This is similar to clinical studies demonstrating that ~26% of young, asymptomatic women display a PCOM phenotype (30); hence the reason PCOM cannot be used as the sole diagnostic criteria for PCOS. We now show that introduction of a WSD alone leads to similar alterations to ovarian SAF morphology in a primate model, that may also progress with T exposure alone. Collectively, these data suggested that consumption of a WSD, possibly via increased adiposity (31), influences the number and health of the SAF cohort, and T exposure with WSD further alters the cohort either directly or via more pronounced changes in metabolism, such as insulin insensitivity (12).

The increase in numbers of total and atretic SAFs in WSD and WSD+T ovaries at menstruation could be due to alterations in the hypothalamic-pituitary-ovarian axis. It is generally accepted that the intercycle rise and subsequent fall in FSH controls the dynamics of SAF growth verses atresia, and selection of the dominant follicle for ovulation at mid-cycle (32). Also, the ratio of LH:FSH appears important; and elevated LH:FSH ratio is generally associated with PCOS (33). Our study initially focused on LH patterns, since an increase in LH pulse frequency was observed in adolescent girls pre-disposed to PCOS, as well as PCOS women (1). Indeed, an increase in LH pulse frequency was observed in our young (4–5 year old) female monkeys by T-treatment compared to cholesterol-treated controls, prior to onset of WSD (34). But, after the diet change and/or further aging (6.5 years old), the LH pulse frequency in the WSD-treated females was similar to that observed in the WSD+T group (12), which is comparable to that observed in control (regular diet) animals in our colony. However, the WSD reduced the amplitude of LH pulses in both groups (12). In our study, serum FSH levels, only measured in daily samples at menstruation, did not differ between WSD (1.0±0.1 ng/ml) and WSD+T (1.1±0.1 ng/ml) monkeys (12), and were comparable to those circulating in control (regular diet) animals in our colony (0.9±0.1 ng/ml, n=16, unpublished data). But, very subtle changes may impact the SAF pool, since Zeleznik and Kubik (35) reported that a 12.5% change in FSH levels fails to support growth and development of smaller antral follicles during the follicular phase. Further studies are ongoing to evaluate the intercycle changes in gonadotropin levels in monkeys during chronic T and diet treatments, and their relationship to SAF dynamics.

Alternatively, alterations in SAF numbers and health could be due to metabolic features associated with the WSD independent of gonadotropins. When secondary follicles from these same WSD and WSD+T-treated ovaries were cultured in an FSH-replete milieu, less than 50% of the follicles survived two weeks in 3D-culture (compared to >90% of control (36)), and those that survived produced minimal AMH and E at the large preantral to small antral stages, respectively. Thus, follicular dysfunction is associated with early “FSH independent” defects and not remedied by exogenous FSH. Metabolic alterations in WSD +/−T females included increased body fat and elevated fasting insulin and glucose levels (12), however reduced insulin sensitivity was only observed in the WSD + T group. Experiments

are planned to evaluate the impact of local metabolic factors, e.g. lipokines, on primate folliculogenesis.

Consumption of the WSD with and without T also caused profound alterations in the overall transcriptome of macaque SAFs. Six of the 8 major patterns of mRNA expression show significant changes in mRNA levels by exposure to the WSD, and two patterns (2 and 5) are almost exclusively altered by consumption of WSD alone with no effect of concurrent T treatment (Figure 3). Treatment with WSD+/−T altered gene products mapping to pathways involved in apoptosis and cell-cycle regulation (Supplemental Tables 3–4, Supplemental File 5), which could relate to the increased numbers of atretic SAFs in the ovary. Although IHC analyses did not detect differences in numbers of granulosa cells expressing p21 in individual SAFs between control and WSD+/−T females, mRNA levels of p21 (CDKN1A) were significantly increased (3 fold) in SAFs isolated from WSD+/−T ovaries (Supplemental Table 5). Since there are higher numbers of p21-postive granulosa cells in morphologically atretic SAFs (Figure 2A and B), which are increased in number in WSD+/−T ovaries (Figure 1D), it is likely that some of the SAFs isolated for mRNA analyses were destined to become atretic. Other major pathways altered by exposure to the WSD+/−T, such as those associated with cancer (Supplemental Tables 3–4, Supplemental File 5), may also play a role in follicle development or atresia. The data extend our observations of metabolic alterations in serum markers and in adipose tissue, to the lipid and carbohydrate metabolic pathways in the SAFs of macaque females consuming the WSD +/− T (12, 13).

Comparison of the SAF transcriptome between WSD and WSD+T identified numerous processes altered by chronic elevation of T. Levels of 714 mRNAs were altered when WSD +T is compared to WSD alone (Figure 3D). Some of these are included in Supplemental Table 5 and Figure 4. Androgen signaling via the AR appears to be similar between WSD and WSD+T groups; this gene product was equally down-regulated compared to expression in standard diet control SAFs. But, expression of the E receptor ESR1 was altered in WSD +T SAFs compared to other groups. This might reflect regulation of ESR1 by chronic T exposure, similar to reports in other macaque tissues (37). Overall, chronic exposure to mildly elevated T appears to ameliorate many of the WSD-induced effects on the SAF transcriptome (Figure 3A–B). In four of the eight expression patterns, T prevents many of the changes to SAF mRNAs induced by WSD, maintaining mRNA expression at or near that of standard diet controls. For example, decreased expression of mRNA for the LHCGR induced by WSD is prevented by concurrent exposure to T (Figure 4C). However, the WSD +T treatment group also shows distinct alterations in mRNA expression from both standard diet controls and WSD alone (Figure 3B, Patterns 7, and 8); hierarchical cluster and PCA analyses (Figure 3C and Supplemental Figure 2) demonstrate that SAF mRNA expression in WSD+T ovaries is markedly different from both standard diet and WSD alone.

It is tempting to speculate that many of the effects of T exposure are independent of dietary changes. This group recently reported that androgens directly promote follicle survival, but inhibit AMH and E production by preantral-to-small antral macaque follicles during 3-D culture (38). Likewise, the two major enzymes contributing to E production, aromatase (CYP19A1) and 17-a hydroxylase (CYP17A1), and AMH mRNA levels were suppressed in SAFs of WSD +T treated animals (Supplemental Table 5). Staining for CYP17A1, also a

specific marker for androgen-producing theca cells in antral follicles, reinforces evidence that the theca layer is relatively sparse and discontinuous in macaque antral follicles (39), compared that in human (40) and rodent follicles. Consumption of WSD +/− T greatly increased the intensity of CYP17A1 staining in the theca layer of SAFs compared to controls, with a wider theca layer more prominent in the WSD + T group. While semi-quantitative IHC analyses for CYP17A1 protein suggests increased expression, mRNA expression of CYP17A1 was suppressed in WSD+/−T SAFs (Figure 4A). This could be an artifact created by isolation of the SAFs out of the ovarian stroma for mRNA analyses. During manual dissection we observed that, compared to control ovaries, the stroma of ovaries from females consuming the WSD regardless of T exposure was less compact and spongy, with follicles not as tightly associated with the stroma (36). Therefore, the theca layer of SAFs of WSD+/−T monkeys might have been more susceptible to destruction or retention in the ovary during follicle isolation. Alternatively, gene transcription may be suppressed whereas protein translation or half-life may be enhanced. Several studies in women report increased CYP17A1 expression in theca cells, as well as elevated levels of androstenedione in follicular fluid, from PCOS women (41). Whether androgens originating from macaque follicles of WSD or WSD+T treated monkeys are elevated in follicular fluid is unknown. However, due to the experimental design of the current study, we cannot distinguish effects due to T alone since WSD was added during the final 1.5 years of treatment. Further experiments are ongoing that will allow distinction of chronic T effects on SAFs with and without consumption of WSD in young adult monkeys.

The ontology Steroid Metabolic Processes (Supplemental Figure 3C), which displayed marked alterations in response to WSD+/− T, could be one factor contributing to altered follicular dynamics and morphology in these ovaries. The decreased level of CYP19A1 mRNA expression could also explain previous reports of reduced serum E2 levels after onset of WSD in these females (12), along with reduced HSD3B2 mRNA levels (Figure 4B). Of note, T levels of WSD-exposed females were not increased by consumption of the high-fat, high sugar diet (12). Thus it is likely that any alterations in SAF morphology and health, related local actions of steroids, are due to increased exogenous androgens and reduced endogenous E. Based on recent studies of preantral-to-small antral follicles during 3-D culture, the loss of E could reduce follicle survival and growth (42), whereas excess androgen could reduce follicular maturation, including E production (38).

Ontology analyses of the transcriptome indicated that numerous processes associated with folliculogenesis and normal ovarian function were altered in SAFs by WSD+/− T treatment, such as anti-inflammatory activity. Increased systemic inflammation is observed in women with PCOS (43), and increased inflammatory processes are also reported in granulosa cells collected from ovulatory follicles during IVM protocols (44). We also report significant changes in mRNA expression of gene products mapping to angiogenesis (Supplemental Figure 4, Supplemental File 5). Women with PCOS tend to over-respond to gonadotropin exposure during ovarian stimulation protocols with increases in several factors controlling angiogenesis, including VEGF (45). The pattern of mRNA expression within this ontology suggests that many of these effects are due to consumption of a high-fat, high caloric diet. Interestingly, while expression of VEGF mRNA was statistically impacted by exposure to WSD+T ($P<0.04$), the fold-change of expression was low, below the 2-fold threshold for

microarray significance (Supplemental Table 5). But a 3-fold increase in mRNA expression of another angiogenic factor, ANGPT2, by WSD+T treatment was noted (Supplemental Table 5). An increase in the ratio of ANGPT2:1 is associated with follicular atresia, and can cause degeneration of the dominant follicle and disruption of ovulatory processes in macaques (46). Further studies will determine if VEGF, ANGPT1 and ANGPT2 levels are altered in the follicular fluid of antral follicles from females exposed to elevated T, a WSD, or WSD+T, which could impact both oocyte quality, ovulation and luteal function.

Many of the altered genomic processes identified in this study are similarly observed in obese and/or PCOS women (47). Several mRNAs associated with oocyte lipotoxicity in rodents and women (27) had altered expression in the SAF cohort of WSD+/−T females (Supplemental Table 5), and overall gene products associated with oogenesis were down-regulated (Supplemental Figure 4) suggesting oocyte quality was altered by consumption of the WSD. One gene product associated with endoplasmic stress, HSPA5 (GRP78), was up-regulated over 4 fold by exposure to the WSD alone compared to standard diet controls (Supplemental Table 5). Other investigators report increased expression of HSPA5 in murine oocytes cultured in lipid-rich follicular fluid (27), in agreement in the current pattern of expression. Likewise, several mRNAs expressing products involved in fatty acid biosynthesis were altered in SAFs of this study, as well as cells from follicles of PCOS women. However, it is important to note that most of the microarray/ genomic data available from women with PCOS are from RNA analyses of cells obtained from aspirates of large, ovulatory antral follicles (28, 29), which are farther along in follicular development than the SAFs analyzed here. More recently, genomic information was reported from women with PCOS by GWAS studies (48, 49). While we did observe changes in AR expression, which displays altered expression in a cohort of women with PCOS (50), there were no changes in mRNA levels of the recently identified PCOS-associated mRNA DENND1A (48). The function of DENND1A is in membrane associated endocytosis and receptor trafficking; there is some evidence that expression of a DENND1A variant increases androgen production in a human theca cell model (51).

In summary, these data strongly suggest that consumption of a WSD in the presence and absence of chronic T exposure impacts not only ovarian SAF numbers and morphology, but also alters the SAF transcriptome. The alterations in ovarian antral follicle morphology, as well as some changes to the SAF transcriptome, are similar to those observed in women with obesity and/or PCOS. However the contribution of chronic elevation of systemic T levels in the absence of WSD consumption during peripuberty and maintained into young adulthood has yet to be determined. Based on previous studies of androgen actions in macaque models (9), the effects of T on SAF gene expression may be compounded when combined with consumption of a diet rich in fats and sugars (WSD). Obesity alone is known to reduce fecundity in women; both the European Society for Human Reproductive Endocrinology (52) and the American Society for Reproductive Medicine (53) released statements and guidelines to physicians to manage reproduction in obese women. Future studies are underway to assess the impact of mildly elevated T independent of WSD on reproductive phenotype, and to determine the relative fertility of WSD+/−T exposed macaque females when compared to standard diet controls. While these data are of translational interest as a

pre-clinical model of PCOS, the larger impact of the effects of diet in general on the ovary and fertility are also important, given the changing diet of women in developed countries.

Supplementary Material

Refer to Web version on PubMed Central for supplementary material.

Acknowledgments

The authors wish to thank the ONPRC Department of Comparative Medicine's Pathology Services Unit (PSU) for their assistance with obtaining ovaries for these projects. We are grateful for the paraffin-sectioning expertise of Barbra Mason in the ONPRC Histopathology - Morphology Research Core. We thank Dr. Jay Wright for donating several antibodies pre-validated in macaque ovarian tissues, and Dr. Ov Slayden for use of his microscope to obtain full-scale pictures of H&E stained rhesus ovaries. The authors would also like to acknowledge the contributions of the OHSU Gene Microarray Shared Resource (GMSR) under the direction of Dr. Chris Harrington (Director) for microarray hybridization and providing access to analysis software.

Funding: P51OD011092 (ONPRC), R21RR030276 (JLC), U54HD071836 and P50HD071836 (RLS), T32HD07133 (WM), K12HD043488 (JX)

References

1. Blank SK, Helm KD, McCartney CR, Marshall JC. Polycystic ovary syndrome in adolescence. Ann N Y Acad Sci. 2008; 1135:76–84. [PubMed: 18574211]
2. Dewailly D, Lujan ME, Carmina E, Cedars MI, Laven J, Norman RJ, et al. Definition and significance of polycystic ovarian morphology: a task force report from the Androgen Excess and Polycystic Ovary Syndrome Society. Hum Reprod Update. 2014; 20:334–52. [PubMed: 24345633]
3. Lee TT, Rausch ME. Polycystic ovarian syndrome: role of imaging in diagnosis. Radiographics. 2012; 32:1643–57. [PubMed: 23065162]
4. Chang RJ, Cook-Andersen H. Disordered follicle development. Mol Cell Endocrinol. 2013; 373:51–60. [PubMed: 22874072]
5. Sheehan MT. Polycystic Ovarian Syndrome: Diagnosis and Management. Clin Med Res. 2004; 2:13–27. [PubMed: 15931331]
6. Huang CC, Tien YJ, Chen MJ, Chen CH, Ho HN, Yang YS. Symptom patterns and phenotypic subgrouping of women with polycystic ovary syndrome: association between endocrine characteristics and metabolic aberrations. Hum Reprod. 2015; 30:937–46. [PubMed: 25662806]
7. Ryan DH, Braverman-Panza J. Obesity in women. J Fam Pract. 2014; 63:S15–20. [PubMed: 24527479]
8. Anderson AD, Solorzano CM, McCartney CR. Childhood Obesity and Its Impact on the Development of Adolescent PCOS. Semin Reprod Med. 2014; 32:202–13. [PubMed: 24715515]
9. Abbott DH, Nicol LE, Levine JE, Xu N, Goodarzi MO, Dumesic DA. Nonhuman primate models of polycystic ovary syndrome. Mol Cell Endocrinol. 2013; 373:21–8. [PubMed: 23370180]
10. Padmanabhan V, Veiga-Lopez A. Sheep models of polycystic ovary syndrome phenotype. Mol Cell Endocrinol. 2013; 373:8–20. [PubMed: 23084976]
11. McGee WK, Bishop CV, Bahar A, Pohl CR, Chang RJ, Marshall JC, et al. Elevated androgens during puberty in female rhesus monkeys lead to increased neuronal drive to the reproductive axis: a possible component of polycystic ovary syndrome. Hum Reprod. 2012; 27:531–40. [PubMed: 22114112]
12. McGee W, Bishop C, Pohl C, Chang J, Marshall JC, Pau FK, et al. Effects of hyperandrogenemia and increased adiposity on reproductive and metabolic parameters in young adult female monkeys. Am J Physiol Endocrinol Metab. 2014; 306:E1292–304. [PubMed: 24735887]
13. Varlamov O, Chu MP, McGee WK, Cameron JL, O'Rourke RW, Meyer KA, et al. Ovarian cycle-specific regulation of adipose tissue lipid storage by testosterone in female nonhuman primates. Endocrinology. 2013; 154:4126–35. [PubMed: 24008344]

14. Bishop CV, Sparman ML, Stanley JE, Bahar A, Zelinski MB, Stouffer RL. Evaluation of antral follicle growth in the macaque ovary during the menstrual cycle and controlled ovarian stimulation by high-resolution ultrasonography. Am J Primatol. 2009; 71:384–92. [PubMed: 19189308]
15. Ting AY, Yeoman RR, Lawson MS, Zelinski MB. In vitro development of secondary follicles from cryopreserved rhesus macaque ovarian tissue after slow-rate freeze or vitrification. Hum Reprod. 2011; 26:2461–72. [PubMed: 21705370]
16. Peluffo MC, Ting AY, Zamah AM, Conti M, Stouffer RL, Zelinski MB, et al. Amphiregulin promotes the maturation of oocytes isolated from the small antral follicles of the rhesus macaque. Hum Reprod. 2012; 27:2430–7. [PubMed: 22593432]
17. Wright JW, Jurevic L, Stouffer RL. Dynamics of the primate ovarian surface epithelium during the ovulatory menstrual cycle. Hum Reprod. 2011; 26:1408–21. [PubMed: 21421660]
18. Cataldo NA, Dumesic DA, Goldsmith PC, Jaffe RB. Immunolocalization of Fas and Fas ligand in the ovaries of women with polycystic ovary syndrome: relationship to apoptosis. Hum Reprod. 2000; 15:1889–97. [PubMed: 10966981]
19. Xu J, Lawson MS, Yeoman RR, Molskness TA, Ting AY, Stouffer RL, et al. Fibrin promotes development and function of macaque primary follicles during encapsulated three-dimensional culture. Hum Reprod. 2013; 28:2187–200. [PubMed: 23608357]
20. Bishop CV, Aazzerah RA, Quennoz LM, Hennebold JD, Stouffer RL. Effects of steroid ablation and progestin replacement on the transcriptome of the primate corpus luteum during simulated early pregnancy. Mol Hum Reprod. 2014; 20:222–34. [PubMed: 24219889]
21. Vartanian K, Slottke R, Johnstone T, Casale A, Planck SR, Choi D, et al. Gene expression profiling of whole blood: comparison of target preparation methods for accurate and reproducible microarray analysis. BMC Genomics. 2009; 10:2. doi:2164-10-2. [PubMed: 19123946]
22. Xu F, Stouffer RL, Muller J, Hennebold JD, Wright JW, Bahar A, et al. Dynamics of the transcriptome in the primate ovulatory follicle. Mol Hum Reprod. 2011; 17:152–65. [PubMed: 21036944]
23. Bishop CV, Satterwhite S, Xu L, Hennebold JD, Stouffer RL. Microarray analysis of the primate luteal transcriptome during chorionic gonadotrophin administration simulating early pregnancy. Mol Hum Reprod. 2011; 18:216–27. [PubMed: 22072816]
24. Doniger SW, Salomonis N, Dahlquist KD, Vranizan K, Lawlor SC, Conklin BR. MAPPFinder: using Gene Ontology and GenMAPP to create a global gene-expression profile from microarray data. Genome Biol. 2003; 4:R7. [PubMed: 12540299]
25. Bogan RL, Murphy MJ, Hennebold JD. Dynamic changes in gene expression that occur during the period of spontaneous functional regression in the rhesus macaque corpus luteum. Endocrinology. 2009; 150:1521–9. [PubMed: 18948396]
26. Bogan RL, Murphy MJ, Stouffer RL, Hennebold JD. Systematic determination of differential gene expression in the primate corpus luteum during the luteal phase of the menstrual cycle. Mol Endocrinol. 2008; 22:1260–73. [PubMed: 18258683]
27. Yang X, Wu LL, Chura LR, Liang X, Lane M, Norman RJ, et al. Exposure to lipid-rich follicular fluid is associated with endoplasmic reticulum stress and impaired oocyte maturation in cumulus-oocyte complexes. Fertil Steril. 2012; 97:1438–43. [PubMed: 22440252]
28. Kaur S, Archer KJ, Devi MG, Kriplani A, Strauss JF III, Singh R. Differential gene expression in granulosa cells from polycystic ovary syndrome patients with and without insulin resistance: identification of susceptibility gene sets through network analysis. The Journal of Clinical Endocrinology & Metabolism. 2012; 97:E2016–21. [PubMed: 22904171]
29. Kenigsberg S, Bentov Y, Chalifa-Caspi V, Potashnik G, Ofir R, Birk OS. Gene expression microarray profiles of cumulus cells in lean and overweight-obese polycystic ovary syndrome patients. Mol Hum Reprod. 2009; 15:89–103. [PubMed: 19141487]
30. Bridges NA, Cooke A, Healy MJ, Hindmarsh PC, Brook CG. Standards for ovarian volume in childhood and puberty. Fertil Steril. 1993; 60:456–60. [PubMed: 8375526]
31. Varlamov O, White AE, Carroll JM, Bethea CL, Reddy A, Slayden O, et al. Androgen effects on adipose tissue architecture and function in nonhuman primates. Endocrinology. 2012; 153:3100–10. [PubMed: 22547568]

32. Zeleznik AJ. Follicle selection in primates: “many are called but few are chosen”. Biol Reprod. 2001; 65:655–9. [PubMed: 11514325]
33. Guastella E, Longo RA, Carmina E. Clinical and endocrine characteristics of the main polycystic ovary syndrome phenotypes. Fertil Steril. 2010; 94:2197–201. [PubMed: 20303485]
34. McGee WK, Bishop CV, Bahar A, Pohl CR, Chang RJ, Marshall JC, et al. Elevated androgens during puberty in female rhesus monkeys lead to increased neuronal drive to the reproductive axis: a possible component of polycystic ovary syndrome. Hum Reprod. 2012; 27:531–40. [PubMed: 22114112]
35. ZELEZNIK AJ, KUBIK CJ. Ovarian Responses in Macaques to Pulsatile Infusion of Follicle-Stimulating Hormone (FSH) and Luteinizing Hormone: Increased Sensitivity of the Maturing Follicle to FSH*. Endocrinology. 1986; 119:2025–32. [PubMed: 3095100]
36. Xu J, McGee WK, Bishop CV, Park BS, Cameron JL, Zelinski MB, et al. Exposure of Female Macaques to Western-Style Diet With or Without Chronic T In Vivo Alters Secondary Follicle Function During Encapsulated 3-Dimensional Culture. Endocrinology. 2014; 156:1133–42. [PubMed: 25545382]
37. Dimitrakakis C, Zhou J, Wang J, Belanger A, LaBrie F, Cheng C, et al. A physiologic role for testosterone in limiting estrogenic stimulation of the breast. Menopause. 2003; 10:292–8. [PubMed: 12851512]
38. Rodrigues JK, Navarro PA, Zelinski MB, Stouffer RL, Xu J. Direct actions of androgens on the survival, growth and secretion of steroids and anti-Mullerian hormone by individual macaque follicles during three-dimensional culture. Hum Reprod. 2015; 30:664–74. [PubMed: 25567619]
39. Hild-Petito S, Stouffer RL, Brenner RM. Immunocytochemical localization of estradiol and progesterone receptors in the monkey ovary throughout the menstrual cycle. Endocrinology. 1988; 123:2896–905. [PubMed: 3197647]
40. Sasano H, Okamoto M, Mason JI, Simpson ER, Mendelson CR, Sasano N, et al. Immunolocalization of aromatase, 17 alpha-hydroxylase and side-chain-cleavage cytochromes P-450 in the human ovary. J Reprod Fertil. 1989; 85:163–9. [PubMed: 2644425]
41. Dumesic DA, Richards JS. Ontogeny of the ovary in polycystic ovary syndrome. Fertil Steril. 2013; 100:23–38. [PubMed: 23472949]
42. Ting A, Xu J, Stouffer R. Differential effects of estrogen and progesterone on development of primate secondary follicles in a steroid-depleted milieu in vitro. Human Reproduction. 2015; 30:1907–17. [PubMed: 26040480]
43. Keskin Kurt R, Okyay AG, Hakverdi AU, Gungoren A, Dolapcioglu KS, Karateke A, et al. The effect of obesity on inflammatory markers in patients with PCOS: a BMI-matched case-control study. Arch Gynecol Obstet. 2014; 290:315–9. [PubMed: 24643802]
44. Schmidt J, Weijdegard B, Mikkelsen AL, Lindenberg S, Nilsson L, Brannstrom M. Differential expression of inflammation-related genes in the ovarian stroma and granulosa cells of PCOS women. Mol Hum Reprod. 2014; 20:49–58. [PubMed: 23900753]
45. Humaidan P, Quartarolo J, Papanikolaou EG. Preventing ovarian hyperstimulation syndrome: guidance for the clinician. Fertil Steril. 2010; 94:389–400. [PubMed: 20416867]
46. Xu F, Stouffer RL. Local delivery of angiopoietin-2 into the preovulatory follicle terminates the menstrual cycle in rhesus monkeys. Biol Reprod. 2005; 72:1352–8. [PubMed: 15703373]
47. Wu LL, Dunning KR, Yang X, Russell DL, Lane M, Norman RJ, et al. High-fat diet causes lipotoxicity responses in cumulus–oocyte complexes and decreased fertilization rates. Endocrinology. 2010; 151:5438–45. [PubMed: 20861227]
48. Shi Y, Zhao H, Shi Y, Cao Y, Yang D, Li Z, et al. Genome-wide association study identifies eight new risk loci for polycystic ovary syndrome. Nat Genet. 2012; 44:1020–5. [PubMed: 22885925]
49. Brower MA, Jones MR, Rotter JI, Krauss RM, Legro RS, Azziz R, et al. Further investigation in Europeans of susceptibility variants for polycystic ovary syndrome discovered in genome-wide association studies of Chinese individuals. The Journal of Clinical Endocrinology & Metabolism. 2014; 100:E182–6. [PubMed: 25303487]
50. Wang F, Pan J, Liu Y, Meng Q, Lv P, Qu F, et al. Alternative splicing of the androgen receptor in polycystic ovary syndrome. Proc Natl Acad Sci U S A. 2015; 112:4743–8. [PubMed: 25825716]

51. McAllister JM, Modi B, Miller BA, Biegler J, Bruggeman R, Legro RS, et al. Overexpression of a DENND1A isoform produces a polycystic ovary syndrome theca phenotype. Proc Natl Acad Sci U S A. 2014; 111:E1519–27. [PubMed: 24706793]

52. Dondorp W, de Wert G, Pennings G, Shenfield F, Devroey P, et al. ESHRE Task Force on Ethics and Law including. Lifestyle-related factors and access to medically assisted reproduction. Hum Reprod. 2010; 25:578–83. [PubMed: 20085914]

53. Practice Committee of American Society for Reproductive Medicine. Obesity and reproduction: an educational bulletin. Fertil Steril. 2008; 90:S21–9. [PubMed: 19007633]

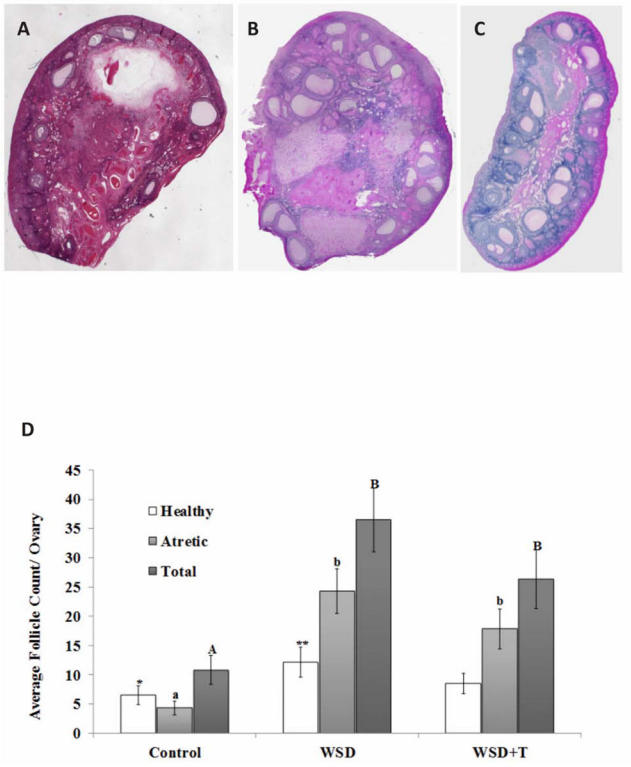

Figure 1.

Upper Panels: Representative H&E-stained sections (5X final magnification) from ovaries of rhesus monkeys consuming a standard diet (Control; Panel A), WSD (Panel B), and WSD+T (Panel C). See text for details.

Lower Panel D. Estimated numbers of SAFs in the ovary from histological analyses (mean ±SEM). See text for details of estimation methods and statistical analyses. Lower case letters denote significant differences ($P<0.05$) in numbers of atretic SAFs between experimental groups, while uppercase letters denote significant differences in total SAFs. Asterisks denote a trend ($P=0.06$) toward difference in healthy SAFs between ovaries of standard diet controls and WSD-fed macaques.

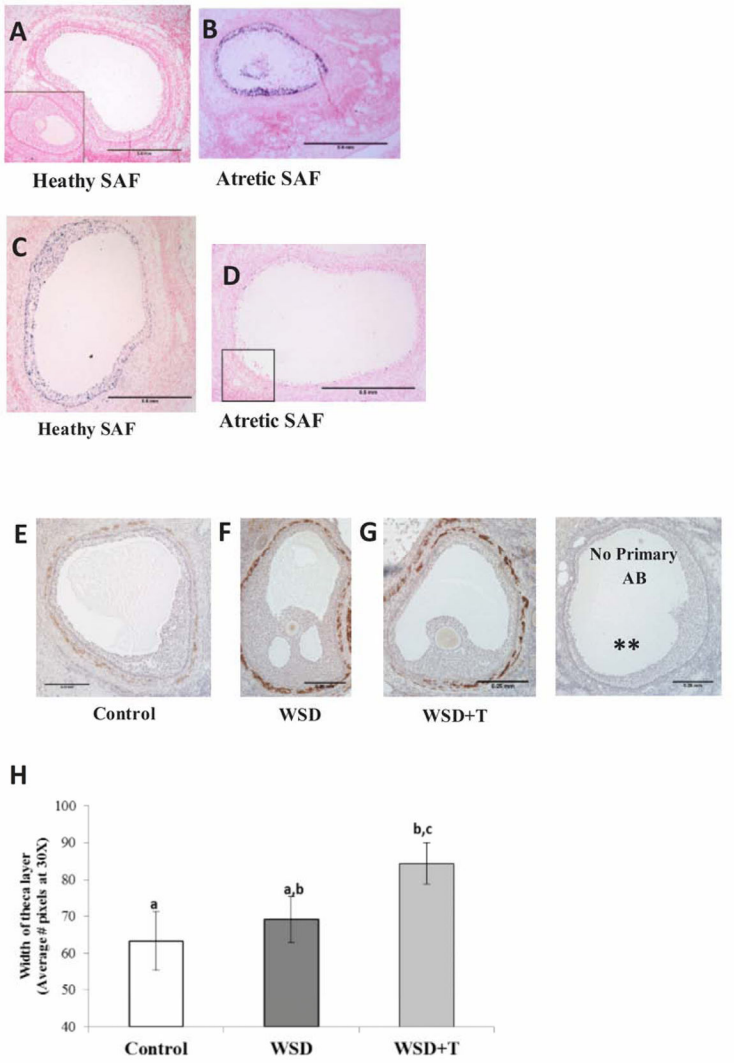

Figure 2.

Immunostaining for the cell-cycle protein cyclin-dependent kinase inhibitor 1A (CDKN1A; p21, dark blue stain) in representative sections of a healthy (Panel A) and atretic (Panel B) SAF in a randomly selected ovary; inset box in A depicts negative control staining (no primary antibody). Scale bar = 0.5mm

Immunostaining for phosphorylated retinoblastoma 1 (pRb, purple stain) in representative sections of a healthy (Panel C) and atretic (Panel D) SAF in a randomly selected ovary; inset box in D depicts negative control staining (no primary antibody). Scale bar = 0.5mm

Immunostaining for CYP17A1 (brown stain) denotes extent of theca layer in representative sections of healthy SAFs in ovaries from standard diet Control (Panel E), WSD (Panel F), and WSD+T (Panel G)-treated monkeys. (** denotes no primary antibody negative control). Scale bar = 0.25mm

Panel H summarizes the quantification of the width of the theca layer in healthy SAFs of macaque ovaries in the three experimental groups (mean±SEM). See text for details of

statistical analyses. Different letters indicate significant differences between experimental groups ($P<0.05$).

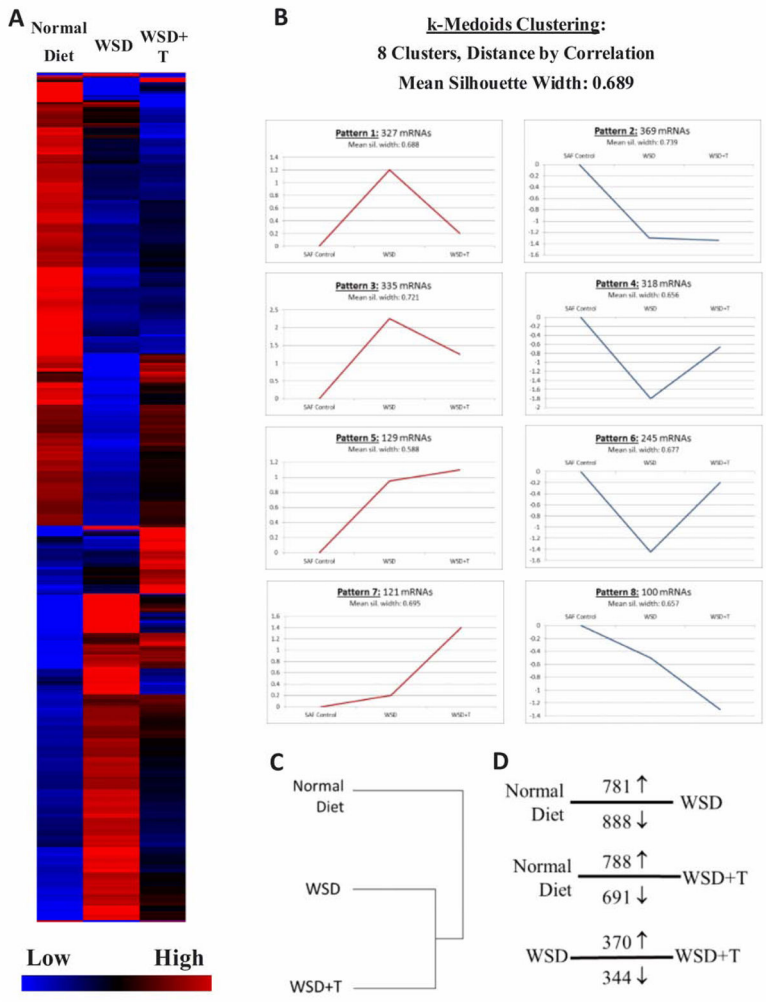

Figure 3.

Panel A. Heat map of 1944 mRNAs whose levels in SAFs were significantly altered by WSD+/−T compared to standard diet controls, with blue color indicating low and red indicating high expression levels. Each column represents relative mRNA levels (indicated by bar on lower right) from each group. See text for details of statistical analyses.

Panel B. k-Medoids clustering analyses using correlation distance identified 8 patterns of mRNA expression changes induced by WSD and WSD+T. Graphs include numbers of mRNAs displaying each pattern of expression. Red graphs show clusters in which mRNAs are initially up-regulated by either WSD and/or WSD+T, and blue graphs denote clusters in which mRNAs are initially down-regulated by either WSD and/or WSD+T.

Panel C. Hierarchical cluster analysis of mRNA samples hybridized to Rhesus Gene Chip microarrays. See text for details of analyses.

Panel D. Results of Pairwise Comparisons between relevant treatment groups showing the number and direction of mRNA changes (↑, increased; ↓, decreased). Lines denote groups compared. See text for details of statistical analyses.

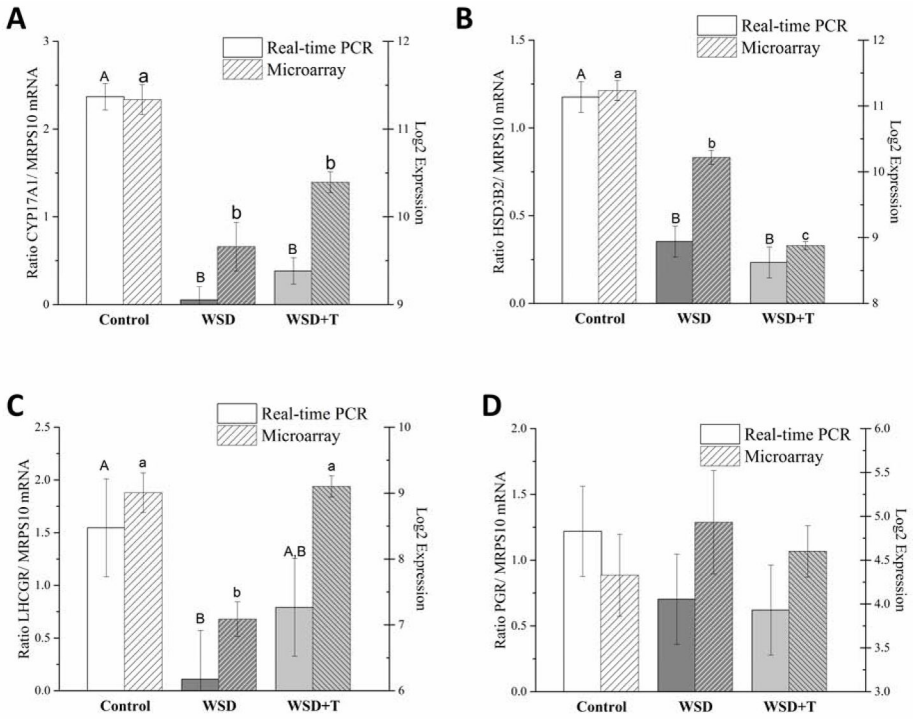

Figure 4.

Real-time PCR validation of mRNA levels for selected gene products of interest based on the microarray data (mean±SEM). Different uppercase letters indicate significant difference in mRNA expression by Real-time PCR, and different lower case letters indicate significant difference in mRNA expression by microarray ($P<0.05$). See text for further details.